Front. Optoelectron. 2012, 5(1): 51–62
DOI 10.1007/s12200-012-0185-x

REVIEW ARTICLE

Spontaneous emission rate enhancement of nano-structured silicon by surface plasmon polariton

Xue FENG, Fang LIU, Yidong HUANG (✉)

State Key Laboratory of Integrated Optoelectronics, Department of Electronic Engineering, Tsinghua University, Beijing 100084, China

Abstract Surface plasmon polariton (SPP) is an attractive candidate to improve internal quantum efficiency (QE) of spontaneous emission (SE) from nano-structured silicon (Si) including nano-porous silicon (NP-Si) and silicon nanocrystal (Si-NC). Since the SPP resonant frequency of common metals, e.g., gold (Au), silver (Ag), copper (Cu), and aluminum (Al), is too high, the SPP resonance has to be engineered to match the luminescence from nano-structured Si. For this purpose, we have proposed and demonstrated three approaches including metal-rich $Au(1-\alpha)$-$SiO_2(\alpha)$ cermet SPP waveguide (WG), compound layer structure WG and metallic grating. In this paper, those approaches are reviewed and discussed. According to the calculated results, such three methods could effectively enhance SE rate from NP-Si or Si-NCs and show potential in developing high efficiency Si based light sources with electric pump.

Keywords spontaneous emission (SE), silicon nanocrystal (Si-NC), surface plasmon polariton (SPP), Purcell effect

1 Introduction

In the past two decades, silicon (Si) photonics attract intensive attention and interest due to good optical properties, low cost of the material and easy manufacturability with standard complementary metal-oxide-semiconductor (CMOS) processes. Furthermore, the use of Si in photonics provides the possibility to merge electronics and photonics in the same chip. Such integrated optoelectronic chips are attractive for both the high computation capability of electronics and the high communication bandwidth of photonics [1]. However, despite the good optical properties, bulk Si has been considered unsuitable for optoelectronic applications due to its indirect electronic bandgap. In the early 1990s, Canham demonstrated visible light emission from porous Si [2], which boosted the research of Si light sources. From that time, there has been much effort on improving the light-emission properties of Si such as nanoporous silicon (NP-Si) [3], erbium doped Si [4], all-Si Raman laser [5] and silicon nanocrystals (Si-NC) [6–9]. Among them, nano-structured Si (NP-Si or Si-NC) has attracted a great interest since intense visible luminescence has been observed at room temperature due to quantum confinement effect [2,3,6–9]. Moreover, stimulated emission and light amplification in Si-NC have also been observed [10]. However, the internal quantum efficiency (QE) of light emission from NP-Si or Si-NC is still not high enough for real applications due to dominant nonradiative recombination. Surface plasmon polariton (SPP) is an attractive candidate to solve such long-standing obstacle [11–15]. The enhanced spontaneous emission (SE) rate of metal SPP waveguide (WG) has been proposed and demonstrated on wide band gap semiconductors, such as GaN/InGaN [11–14] and ZnO [15]. The dispersion of such a SPP WG yields large density of states (DOS) for photon near the resonant frequency and according to Fermi's golden rule, the radiative recombination and SE rate are enhanced correspondingly. This is the so-called Purcell effect [16] that modifies the SE by engineering the dispersion. Unfortunately, the SPP resonant frequency of common metals, e.g. gold (Au), silver (Ag), copper (Cu), and aluminum (Al), is so high that this method is not so effective for nano-structured Si unless the average size of NP-Si or Si-NC is very small. In order to apply metal SPP enhancement for Si light sources, the SPP resonant frequency should be engineered to match the luminescence from nano-structured Si.

In order to apply SPP enhancement on nano-structured Si, we proposed several approaches in the last five years. Firstly, a kind of metal-rich $Au(1-\alpha)$-$SiO_2(\alpha)$ cermet nanowaveguide was proposed in our previous work [17]. By properly choosing the component of the cermet, the SPP-like dispersion of the nanowaveguide can be engineered so that the SE of NP-Si is greatly enhanced.

Received August 23, 2011; accepted September 13, 2011

E-mail: yidonghuang@tsinghua.edu.cn

To obtain further larger region enhancement, we proposed double-layer SPP WG structure [18]. Comparing double layer with mono-layer SPP WG, the electromagnetic field could be concentrated more in the active layer so that higher Purcell factors (PFs) could be achieved.

With the metal-rich cermet, we found that only Au can be used to obtain enhanced luminescence for emission energy below 2.0 eV since the SPP resonant frequency of Au is relatively low. Then we introduced an Ag-poor cermet layer into SPP WG structure [19], which is so-called compound layer structure. Due to large permittivity of Ag-poor cermet and its unique dispersion characteristic, DOS can be enhanced at the frequency much lower than the plasmon frequency of Ag. By properly choosing the component of the Ag-poor cermet, the SPP resonant frequency can be engineered to match the central emission of Si-NC. Therefore significant SE rate enhancement of Si-NC can be realized by using Ag instead of Au.

It is well known that Cu, rather than Au and Ag, is the mainstay metal material in microelectronics chips. If Cu can be adopted to provide SPP enhancement of light emission from Si light sources, it would be a notable promotion for integrating Si emitters on microelectronics chip. Then we proposed metallic grating to enhance the SE rate of Si-NC [20,21]. Due to SPP band gap (SPPBG) effect on metallic grating, the band edge (BE) frequency of SPPBG can be engineered within luminescent frequency range of Si-NCs with proper grating period. The calculated results indicate that the common metals such as Au, Ag, Al and Cu can be used to enhance the SE from Si-NCs with grating structure. It should be noticed that the Cu grating can be employed to overcome the frequency mismatch between SPP resonance and Si-NCs luminescence. Since Cu is the most commonly adopted metal in integrated-circuit (IC) manufacturing, this method provides a promising approach to realize Si light sources on chip.

In this paper, the aforementioned three kinds of approaches for SPP enhanced SE from nano-structured Si are reviewed and discussed. It is organized as follows: in Section 2, fundamentals of guided SPP mode and Purcell effect are provided; in Section 3, the proposed method of metal-rich Au$(1-\alpha)$-$SiO_2(\alpha)$ cermet nanowaveguide and double-layer structure are presented; in Section 4, the results for Ag/Ag-poor cermet compound layer structure are presented; in Section 5, the proposed Cu-Si_3N_4 grating is discussed with Au, Ag and Al-Si_3N_4 gratings; Section 6 provides a summary.

2 Fundamentals of guided SPP mode and Purcell effect

In this session, the fundamental properties of guided SPP mode and Purcell effect will be briefly summarized while more details could be found in Refs. [11,17–22].

SPP is a surface electromagnetic wave that is transverse magnetic polarized (transverse magnetic (TM) or p-polarized) and propagates along the metal-dielectric interface and the amplitude decays exponentially with increasing distance into each medium from the interface. The electromagnetic field of a SPP mode could be obtained from the solution of Maxwell's equations in each medium, and the associated boundary conditions. As shown in Fig. 1, we consider the simplest system consisting of a dielectric material, characterized by an isotropic, real, positive permittivity ε_D, in the half-space $z>0$, and a metal, characterized by an isotropic, frequency-dependent permittivity function $\varepsilon_M(\omega)$ in the half-space $z<0$. In our reference coordinate system shown in Fig. 1, the magnetic field of TM SPP mode contains the field components perpendicular to the symmetry plane, i.e., the y component. Since the interface is symmetrical along y axis, the electromagnetic field will also be symmetrical along y axis and can be obtained by using Maxwell's equations as:

$$H_y(x,z|\omega)=\begin{cases} A\exp(\mathrm{i}k_x x-\gamma_D z-\mathrm{i}\omega t), z>0, \\ B\exp(\mathrm{i}k_x x+\gamma_M z-\mathrm{i}\omega t), z<0, \end{cases} \tag{1a}$$

$$E_x(x,z)=-\frac{\mathrm{i}c}{\omega\varepsilon}\frac{\partial H_y}{\partial z}, \tag{1b}$$

$$E_z(x,z)=\frac{\mathrm{i}c}{\omega\varepsilon}\frac{\partial H_y}{\partial x}, \tag{1c}$$

where, ω is the angular frequency of SPP mode, k_x is wave vector along x direction and γ_D/γ_M determine the decay of the electromagnetic field with increasing distance from the surface to dielectric/metal material while the relations of them are

$$\gamma_D^2=k_x^2-\varepsilon_D\left(\frac{\omega}{c}\right)^2, \tag{2a}$$

$$\gamma_M^2=k_x^2-\varepsilon_M(\omega)\left(\frac{\omega}{c}\right)^2, \tag{2b}$$

then, with the boundary condition at $z=0$, one can get

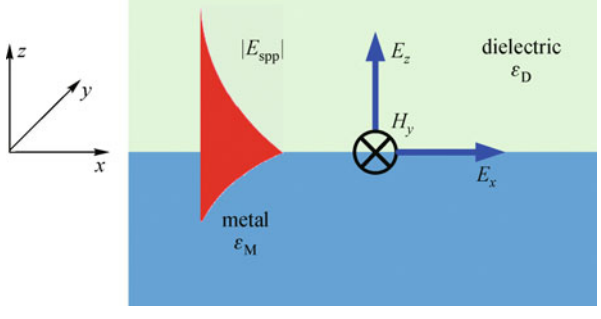

Fig. 1 Schematic of SPP at metal-dielectric interface and reference coordinate system

$$A = B,\ A\frac{\gamma_D}{\varepsilon_D} = -B\frac{\gamma_M}{\varepsilon_M(\omega)}, \tag{3}$$

obviously, Eq. (3) has a nontrivial solution only when ε_M is negative. It is just the physical origin of SPP mode existing at metal-dielectric interface. Physically, one can understand it as photons coupled to collective excitations of conduction electrons near a metal surface. Furthermore, if both sides of Eq. (3) are squared, an explicit expression for the wave vector k_x of the SPP mode as a function of its frequency [22]:

$$k_x = \frac{\omega}{c}\sqrt{\frac{\varepsilon_D\varepsilon_M(\omega)}{\varepsilon_D + \varepsilon_M(\omega)}}, \tag{4}$$

after the dispersion relation is obtained, the electromagnetic field of SPP mode could be calculated by Eq. (1) with $A = B$. Then the SE rate Γ_{sp} can be deduced from Fermi's golden rule:

$$\Gamma_{sp} = \frac{2\pi}{\hbar}|\langle f|\boldsymbol{d}\cdot\boldsymbol{E}|i\rangle|^2\rho(\hbar\omega), \tag{5}$$

where $\langle f|\boldsymbol{d}\cdot\boldsymbol{E}|i\rangle$ is the dipole emission matrix element, $\boldsymbol{d}$ is the electro-hole pair dipole moment, and $\rho(\omega)$ is DOS for photon $\rho(\omega) = k_x\frac{dk_x}{d\omega}$. To evaluate Γ_{sp}, $\boldsymbol{E}$ should be normalized to a half-quantum of zero point fluctuations. In the case of SPP mode, the emitted photons from active dielectric material, as a result of the recombination of electron-hole pair, will be coupled directly to the guided SPP mode instead of free space [11]. Due to the different dispersion relationships of the light in the WG and free space, the DOSs in the two cases are different. Purcell predicted the modification of SE by engineering the DOS, and the PF can be defined as [11]:

$$\begin{aligned}\mathrm{PF} &= \frac{\Gamma_{sp}}{\Gamma_{sp} + \Gamma_{free}} \\ &= 1 + \frac{\pi c^3 E_0(z)^2}{\sqrt{\varepsilon_D}\omega^2\int_{-\infty}^{+\infty}[\partial(\varepsilon\omega)/\partial\omega]E_0(z)\mathrm{d}z}k_x\frac{dk_x}{d\omega},\end{aligned} \tag{6}$$

where Γ_{free} is the SE rate without the cermet WG, $E_0(z)$ is the un-normalized electrical field of the guided SPP mode. Obviously, PF is related to the position of active material along z axis. Especially, PF decays along z direction with $E_0(z)$ as shown so that significant SE rate enhancement can be achieved only near the interface.

Till now, we have introduced some basic but important principles for guided SPP mode and Purcell effect. Although the presented system is simplest, it is very similar to a real and more complicated WG. In the followed session, we will demonstrate the SE rate enhancement for some different SPP WG structures with the same theoretical frame as presented in this session.

3 SPP enhancement on metal-rich cermet WG

In our previous work [17], aiming at improving the internal QE from NP-Si, we proposed a device structure with a metal-rich Au($1-\alpha$)-SiO_2(α) cermet WG. A schematic structure of the porous Si with a cermet WG is shown in the inset of Fig. 2. The active layer is the NP-Si on the Si substrate, which can be prepared by electrochemical etching. On the top of NP-Si is the Au($1-\alpha$)-SiO_2(α) cermet WG with the thickness of h. The structure can be considered as a three-layer model: the air, Au($1-\alpha$)-SiO_2(α) cermet and NP-Si. The electromagnetic field of such structure can be solved by modifying Eqs. (1) and (2) with multilayer model [17]. The permittivity of NP-Si is assumed to be $\varepsilon_D = 4$, which is between air ($\varepsilon_D = 1$) and Si ($\varepsilon_D = 11.6$). As the permittivity of the cermet strongly depends on its component, i.e., the SiO_2 volume fraction α, it is possible to design and engineer the desired dispersion relationship by controlling α. With the effective medium theory with Bruggeman's formula [23], the permittivity of cermet (ε_{CM}) could be calculated:

$$(1-\alpha)\left(\frac{\varepsilon_{Au}-\varepsilon_{CM}}{\varepsilon_{Au}+2\varepsilon_{CM}}\right) + \alpha\left(\frac{\varepsilon_{SiO_2}-\varepsilon_{CM}}{\varepsilon_{SiO_2}+2\varepsilon_{CM}}\right) = 0, \tag{7}$$

where ε_{Au} and ε_{SiO_2} are the permittivity for Au and SiO_2. In the case of small α, i.e., the cermet is metal rich, it is reasonable to suppose that its optical property can still be described by the Drude model $\varepsilon_{CM}(\omega) = \varepsilon_\infty\left[1 - \frac{\omega_p^2}{\omega(\omega+i\Gamma)}\right]$. The calculated ε_{CM} by Eq. (2) is fitted by using the Drude model, and two important parameters, namely, plasmon frequency ω_p and dielectric constant at high frequency ε_∞, are shown in Fig. 2 as a function of α. From Fig. 1, one can see that the plasmon frequency ω_p is decreased as a result of doping SiO_2.

After the permittivity of cermet is obtained, the dispersion relationship of the WG could be obtained with various volume fractions as shown in Fig. 3(a). The thickness of the WG, h, is supposed to be 10 nm. As Au dominates in the cermet, the property of the WG is surface-plasmon-like with two branches, i.e., the symmetric (S) branch and the anti-symmetric (AS) branch, respectively. The light lines in air (the gray line) and in NP-Si (the black line) are also shown. An important feature in Fig. 3(a) is that the resonant frequency decreases as the SiO_2 volume fraction α increases. A typical photoluminescence (PL) spectrum of the NP-Si is shown in the inset of Fig. 3(a), which centers at $\hbar\omega = 1.718$ eV. The shaded area corresponds to the frequency range between two half-maxima. As the frequency of the S mode is much higher than that of NP-Si luminescence, we ignore this mode and discuss the AS mode only. By using Eq. (6), the PF could

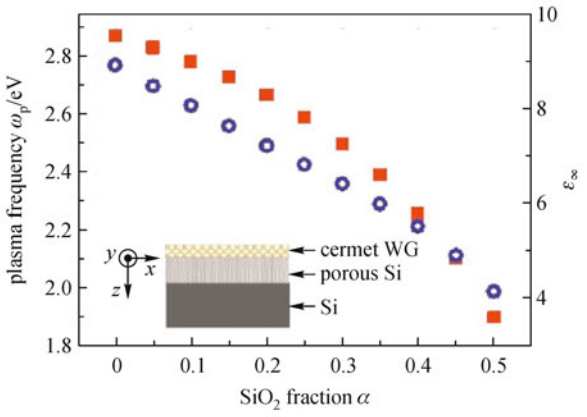

Fig. 2 Dependence on SiO_2 volume fraction α of plasmon frequency ω_p (square) and high frequency dielectric constant ε (circle) in Drude model of metal-rich cermet. Inset: schematic structure of nanoporous Si layer with a Au(1 –α)-SiO_2(α) cermet WG

also be calculated and the results are shown in Fig. 3(b). It can be seen from Fig. 3(b) that the maximum of PF is red-shifted as α increases. This red-shift is very important because it increases the PF at lower frequencies, which is long covered for increasing the SE rate from NP-Si. For example, the shaded area in Fig. 3(b) represents the main body of the luminescent spectrum (see the inset of Fig. 3 (a)) and one can see that PF associated with a cermet WG ($\alpha = 20\%$) is much larger than that with a pure Au WG. To illustrate this point more clearly, fixing the photon frequency at $\hbar\omega = 1.718$ eV, the PF as a function of α is also shown in the inset of Fig. 3(b). As a comparison, one can see that with pure Au, the PF is only 50 while the PF can be increased to 210 by doping 20% SiO_2.

Proposed device structure with a cermet nanowaveguide makes the radiative recombination process dominate inside a NP-Si layer. Without the WG, the nonradiative recombination process still dominates inside NP-Si, although quantum confinement effect does enhance the radiative one. To give a concept of order, the typical nonradiative lifetime of careers in NP-Si is $\tau_{nr} = 1$ μs and typical radiative one is $\tau_r = 30$ μs; these will vary with temperature, doping, etc., though. The internal QE η_{int} can be generally expressed as:

$$\eta_{int} = \frac{PF\tau_r^{-1}}{PF\tau_r^{-1} + \tau_{nr}^{-1}}, \quad (8)$$

where τ_r and τ_{nr} are the radiative and nonradiative lifetimes, respectively.

To make a clear comparison, η_{int} (the case that $\alpha = 20\%$ as an example) with the cermet WG and without the WG are illustrated as a distribution along z in Fig. 4. One can see that η_{int} is greatly improved and always larger than that without the WG within the entire transversal extension of the guided mode inside the NP-Si. Especially, in the layer that $z < h_c$ (about 20 nm, which is much thicker than the thickness of WG $h = 10$nm), $\eta_{int} > 50\%$ and $\tau_r^{enhanced} < \tau_{nr}$, which means that radiative recombination dominates.

In the aforementioned part, only one cermet layer on top of active material is considered. In order to obtain more effective enhancement of Si-NC, a double layer structure was further proposed based on the original idea of adopting Au-rich cermet [18]. Figure 5 shows the proposed double layer structure, the monolayer is also presented for comparison. Active layer can be considered as Si quantum dots embedded in SiO_2 matrix (indicated by SiO_x, $x < 2$)

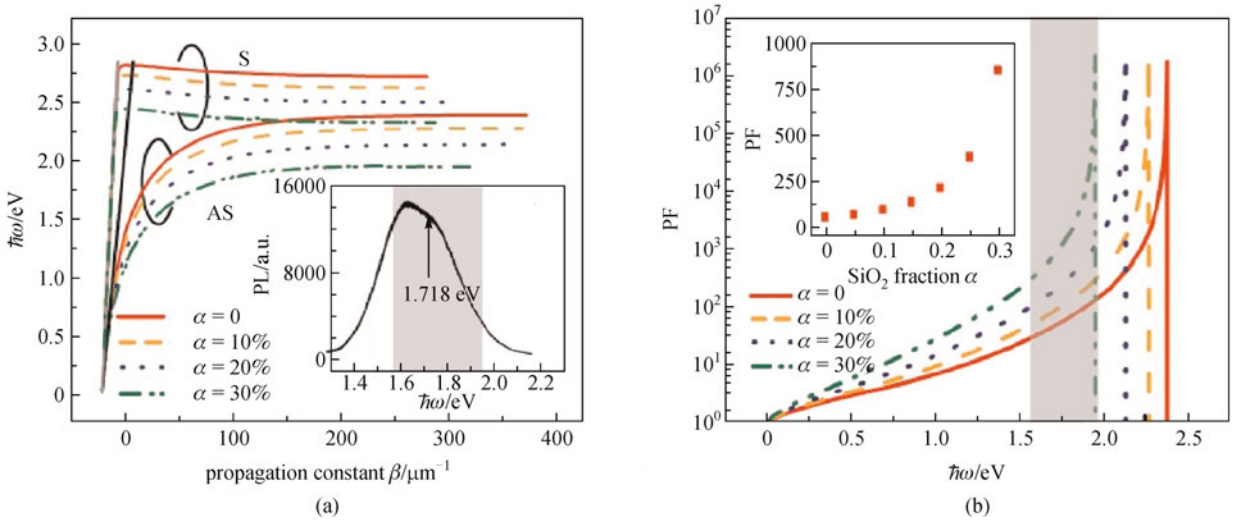

Fig. 3 (a) Dispersion of Au(1 –α)-SiO_2(α) cermet WG with different components. Inset: typical PL spectrum of NP-Si. Shaded area corresponds to frequency range between two half-maxima; (b) PF with different components α versus photon energy $\hbar\omega$. Inset: increase of PF with the increase of SiO_2 volume fraction α, fixing the photon energy at 1.718 eV

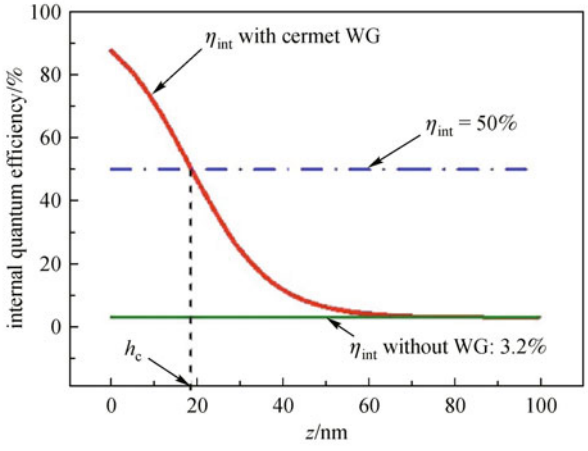

Fig. 4 Distributions of internal QE η_{int} with and without cermet WG

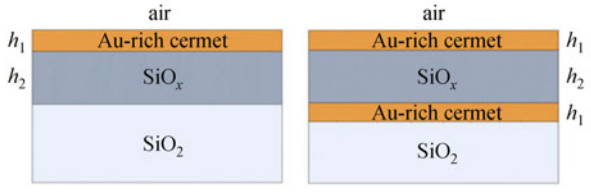

Fig. 5 Schematic of monolayer and double layer structures

with thickness of h_2 and refractive index of 1.71. By inserting another Au-rich cermet film at the SiO_x/SiO_2 interface, monolayer can be modified to the double layer structure. For a concrete example, Au$(1-\alpha)$-$SiO_2(\alpha)$ cermet was chosen here. To simplify the discussion, we set two Au-rich cermet films of the double layer structure with the same thickness of h_1 and the same SiO_2 fraction α.

Figure 6 shows the dispersion curve of the monolayer and double layer structure with $h_1 = h_2 = 30$ nm and different SiO_2 fraction ($\alpha = 0$, 0.2). Only the lowest modes of each structure are considered here because they dominate the power dissipation of dipole source closed to metal surface(s). It is can be seen that, increasing the fraction α can lower the SPP resonant frequency and flat the dispersion curve to raise the DOS in relative low frequency region, which in the case of monolayer structure. For typical Si-NC, the luminescence wavelength region is from 600 to 900 nm ($\hbar\omega = 2.07 - 1.38$ eV), which is very similar to the NP-Si. In such luminescence range, the dispersion curves of the double layer structure are more flat than that of mono-layer. This phenomenon can be explained from the view point of coupled mode theory: the mode of double layer can be treated as the lower frequency branch produced by coupling between the modes of two mono-layer WGs, and the frequency splitting flats the dispersion curve of lower branch, which yields larger DOS and is beneficial to PF improvement. Due to the transversal exponent-evanescent property of the guided mode in the active region, electric field decrease quickly along the direction perpendicular the interface in the mono-layer structure; only the region near the Au cermet/SiO_x interface can obtain evident enhancement. While in the double layer structure, exponent-evanescent property is not so serious due to the influence of the other Au cermet/SiO_x interface, which will result in noticeable improvement in PF for the whole active region. Here, we fixed the photon frequency at $\hbar\omega = 1.654$ eV (equivalent to the wavelength at 750 nm), and then calculated the $|E|^2$ distribution of the monolayer and double layer structures. The results are shown in Figs. 6(a) and 6(b), respectively. Although the field will evanescently decay from the interface, if the distance is small enough, electric field can still keep a relatively high value. It can be seen from Fig. 6(b) that, due to the effect of the double layer structure, electric field mostly concentrates in SiO_x active region. Then much smaller modal volume, combining with DOS enhancement, results in a noticeable improvement of PF. For the case of $\alpha = 0$ and 0.2, PF (over entire SiO_x active region) increases from no more than 4 and 6 to all above 17 and 21, respectively.

In summary, we have proposed and theoretically demonstrated the enhancement of SE from a NP-Si or Si-NC layer with a metal-rich Au$(1-\alpha)$-$SiO_2(\alpha)$ cermet WG. The dispersion can be engineered by controlling the component of the WG so that the DOS can be tuned to be very large at the luminescent frequencies. Therefore SE can be greatly enhanced due to Purcell effect and the internal QE is greatly increased. Some detailed discussions could be found in Refs. [17,18].

4 SPP enhancement on metal-poor cermet WG with compound structure

In Session 3, we have demonstrated the so called metal-rich cermet to lower the plasmon frequency by doping dielectric into metals. However, to obtain enhancement for luminescence from NP-Si or Si-NC ($\hbar\omega$<2.0 eV), only Au, which has relatively low plasmon frequency, can be used with such method. If adopting other metals, whose plasmon frequency are relative high, the dielectric doping fraction should be high so that the cermet is metal-poor and dielectric like with positive real part of permittivity in some frequency region. In order to use such metal materials with higher plasmon frequency, we proposed a compound structure SPP WG [19], where an Ag-poor cermet layer was introduced into SPP WG structure as shown in Fig. 7.

For the proposed structure as shown in Fig. 7(a), the active layer is the Si-rich nitride (SRN), which can be prepared by plasma-enhanced chemical vapor deposition. On the top of the SRN is an Ag film, covered by a thin Ag-poor cermet layer consisted of Ag$(1-\alpha)$-$Si_3N_4(\alpha)$, where

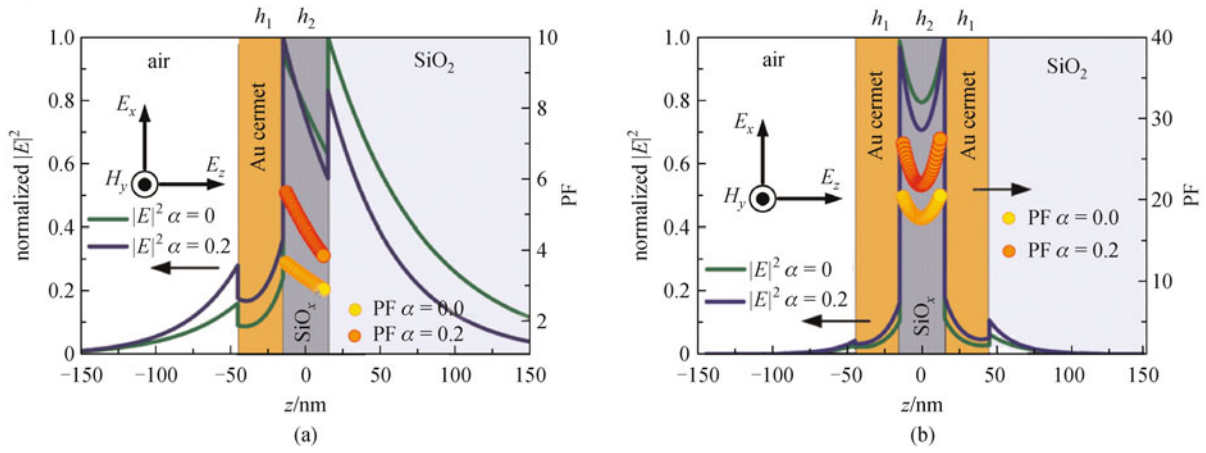

Fig. 6 $|E|^2$ and PF distributions in (a) monolayer; (b) double layer; SP WG ($h_1 = h_2 = 30$ nm). The calculated $|E|^2$ field and PF are shown as lines and circles, respectively. And different colors indicates two components of $\alpha = 0$ and 0.2

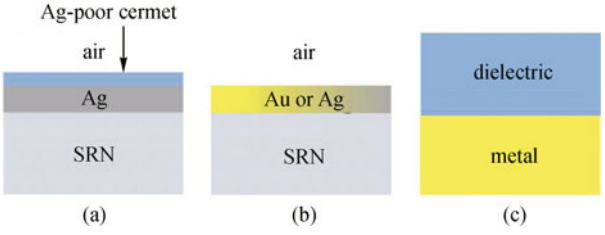

Fig. 7 (a) Ag/Ag-poor cermet SPP WG; (b) SPP WG with pure Au or Ag film; (c) two-layer SPP WG

the Si_3N_4 volume fraction α exceeds 0.5. Such structure is so called compound layer structure. For comparison, the structures without Ag-poor cermet and the simplest two layers SPP WG are also presented as Figs. 7(b) and 7(c).

In the case of $\alpha > 0.5$, the cermet is Ag-poor and dielectric like with positive real part of permittivity in some frequency region. Furthermore, the cermet permittivity and its dispersion are both several times larger than that of the doping dielectric, which are the key factors to notably increase the DOS. Because the DOS is proportional to $k\mathrm{d}k/\mathrm{d}\omega$, large value of DOS can be obtained near the resonant frequency where the dispersion curve is flat. Figure 8 is the calculated dispersion relationship of Ag/Ag-poor cermet layer (Fig. 7(a)), compared with the pure Au or Ag film without Ag-poor cermet (Fig. 7(b)). It can be seen that in Fig. 8(a), there is only one resonant frequency for pure Au or Ag film. Even though the resonant frequency of Au film is lower than that of Ag film due to different plasmon frequencies of Au and Ag, resonant frequency of Au film is still higher than 2.0 eV. It is noticed that the Ag/Ag-poor cermet layer has two resonant frequencies, one is almost the same with Ag film, and the other is much lower, even lower than that of Au film. Furthermore, SPP resonant frequency of the Ag/Ag-poor cermet layer shifts with different components, i.e., the Si_3N_4 volume fraction α. As shown in Fig. 8(b), it is possible to engineer the SPP resonant frequency in a wide region to match the Si-NC luminescence.

Large value permittivity and the unique dispersion of the Ag-poor cermet are the key factors to notably increase the DOS. As a concrete example, the photon frequency is fixed at $\hbar\omega = 1.7106$ eV (equivalent to the wavelength at 725 nm), and the corresponding calculation results of the DOS is shown in Fig. 9(a). It can be seen that thicker Ag-poor cermet layer is suitable to obtain larger DOS. To concisely explain this conclusion, we take the two-layer structure (Fig. 7(c)) for example, where the metal layer and the dielectric layer are both with infinity thickness. Generally, it is considered that the dispersion of dielectric is too small to influence the DOS. However, dispersion of dielectric-like cermet, the value of $\mathrm{d}\varepsilon_D/\mathrm{d}\omega$, is much higher than that of traditional dielectric. Therefore its influence to DOS should no longer be neglected in this case. It should be figured out that, when the metal is fixed, large values of ε_D and $\mathrm{d}\varepsilon_D/\mathrm{d}\omega$ will both increase the DOS. For a more complex structure, as shown Fig. 7(a), we can consider that the multilayer dielectric/cermet as one layer material with equivalent permittivity which is affected by the permittivity and field filling factors of each layer. Thus, introducing Ag-poor cermet into structure would still result in positive effect to DOS enhancement. It is also noticed that increasing the thickness results in the growth of DOS. It can be considered that increasing thickness means increase in proportion of Ag-poor cermet, as well as the equivalent permittivity and its dispersion, which finally reflects on the growth of DOS. At the mean time, when thickness exceeds a certain value, increase in the thickness of Ag-poor cermet could not obtain further significant DOS enhancement. In this situation, field filling factor of Ag-poor cermet is large enough, and the influence of Ag-poor cermet layer has already taken the major part of multilayer. Thus, several dozen nanometers thickness of Ag-poor cermet layer is totally enough for the DOS enhancement.

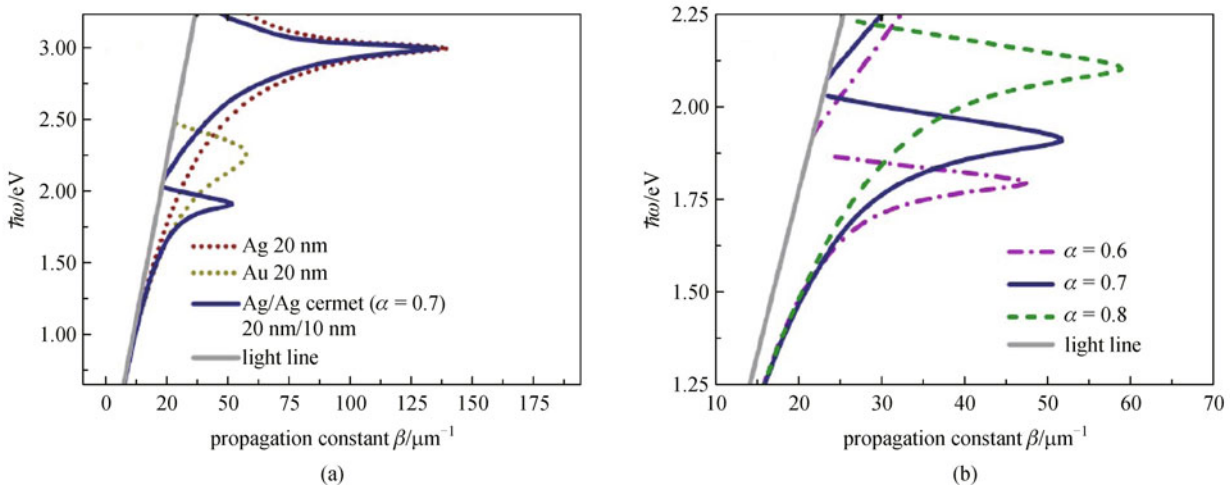

Fig. 8 (a) Dispersion of Au, Ag, Ag/Ag-poor cermet SP WG; (b) dispersion of the Ag/Ag-poor cermet SP WG with different Si_3N_4 fractions

Furthermore, the corresponding PFs are also calculated and shown in Fig. 9(b). As a concrete example, emitting dipole is assumed 5 nm away from the interface of metal/SRN, and the photon frequency is still fixed at $\hbar\omega =$ 1.7106 eV (equivalent to the wavelength of 725 nm). It can be seen that the tendency of PF is different from that of DOS. The Si_3N_4 fractions, corresponding to the maximum value of DOS and PF, respectively, are not the same, and this phenomenon is more evident with thicker Ag-poor cermet layer. This is because the field distribution also affects the value of PF, according to Eq. (6). Over thick Ag-poor cermet layer reduces the field concentration in active layer, which is harmful for PF. Thus, there is a tradeoff on the thickness of Ag-poor cermet layer. In our case, the optimization thickness is about 15 nm.

In our previous work [17], it is figured out that high volume fraction of dielectric, which lowers the resonant frequency and realizes large region tuning, will increase the resistivity of metal rich cermet and be harmful for electric performance of devices. On the other hand, in the structure we proposed here, even the Ag-poor cermet has very large resistivity; the lower Ag layer can still serve as the electrode for Schottky type Si light source with very good conductivity. Namely, the compound layer structure provides an approach that we can optimize the optical performances (SPP mediated enhancement) and electric

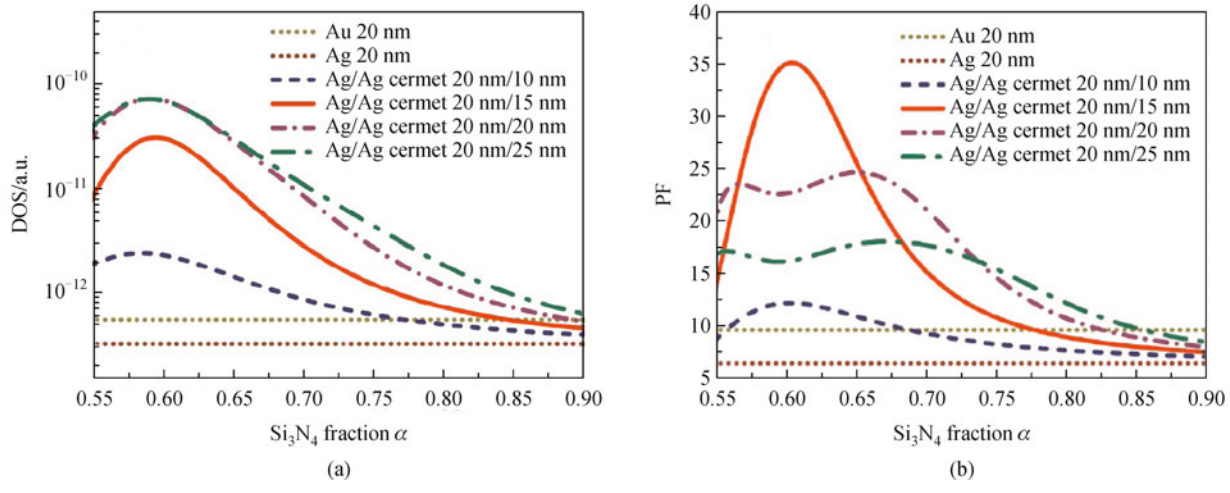

Fig. 9 Dependence on Si_3N_4 fraction α of (a) DOS; (b) PF with different thicknesses of Ag-poor cermet layer, fixing the photon energy at 1.7106 eV (equivalent to the wavelength at 725 nm). The yellow and wine dot lines are the reference results of 20 nm thick Au and Ag film, respectively

behavior (conductivity) separately, in a wide frequency range.

5 SPP enhancement on metallic grating

In Sections 3 and 4, we have demonstrated two approaches based on metal rich/poor cermet SPP WG. In this session, we will demonstrate a different but more flexible approach based on metallic gratings to enhance the SE from Si-NC. As shown in Fig. 1, the shape of spatially periodic metal-dielectric interface, i.e., one dimensional metallic grating, is described as $z = s(x)$ with period of a. The interface consists of dielectric in the region $z > s(x)$ and metal in the region $z < s(x)$. The metal is characterized by a real, isotropic, and frequency dielectric function.

When SPP wave propagates on such a periodic interface, two standing wave solutions of SPP modes can be found with respect to the peaks and troughs of the interface. Therefore the dispersion curve splits into two branches. Just like "photonic band gap" (PBG) in spatially periodic dielectric structures called "photonic crystals" [24,25], SPPBG can also occur, where propagation of SPP mode over certain range of frequency is forbidden [25]. At the BE-frequency, the DOS for photon is very large and the SE rate can be greatly enhanced [11–15]. Since the BE-frequency only depends on the parameters of the metallic grating (period, depth, etc.), large DOS and SE rate enhancement can be achieved within a large frequency range by properly engineering the periodic structure in spite of the applied materials. In other words, the mismatch between SPP resonance and luminescence of Si-NCs can be overcome by adopting the metallic grating.

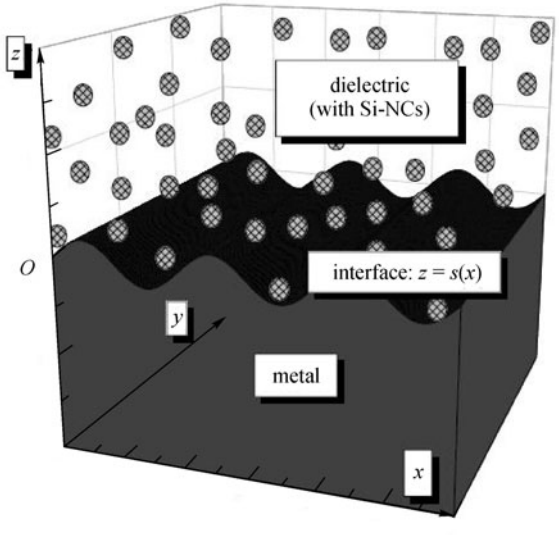

Fig. 10 Schematic cylindrical periodic dielectric-metal interface and reference coordinate system. Interface consists of dielectric in the region $z > s(x)$ and metal in the region $z < s(x)$

For metallic grating, the SPP modes solutions and the formula of PF are different from to those described in Section 2. In our previous work, we have proposed a combination method to obtain the numerical solution of SPP mode propagating on a cylindrical periodic dielectric-metal interface, including both of dispersion relation and field distribution [26]. Moreover, we have deduced the PF formula for the case of one dimensional metallic grating [20,21]. The details could be found in the mentioned references and here only some important results are presented.

In the calculation, we assume that the Si-NCs are embedded in Si nitride (Si_3N_4). The permittivity of Si_3N_4 is assumed as $\varepsilon_D = 4$. The metallic grating was assumed as sinusoidal shape $s(x) = d\sin(2\pi/ax)$ with period a and depth $d = 0.1a$. After the metal material and period of the metallic grating are determined, the dispersion relation $k(\omega)$ and the electromagnetic field distribution $\boldsymbol{E}(x, z)$ could be obtained by our proposed combination method [26]. Figure11 shows calculated dispersion relations for Cu-Si_3N_4 grating with the period from a = 90 to 140 nm. As a reference, the dielectric light line (Si_3N_4) and dispersion curve of flat Cu-Si_3N_4 interface are also plotted with dashed and solid line, respectively. The energy band gap can be observed clearly. There are two branches for the dispersion curves of sinusoidal shaped interface while one is higher than that of flat interface and the other is lower. It can be found that the BE-frequency for lower branch is varied from $\hbar\omega = 1.92$ to 1.58 eV with increasing period. Such results indicate that the BE-frequency of SPPBG can be engineered according to Si-NCs luminescence with proper grating period. Additionally, it should be noticed that there is only one branch for a = 90 nm. The reason is because the solutions for the higher branch are beyond the plasmon frequency ($\hbar\omega_p = 2.855$ eV).

In principle, both the lower and higher branches could be applied for SPP enhancement. In Fig. 11, it can be

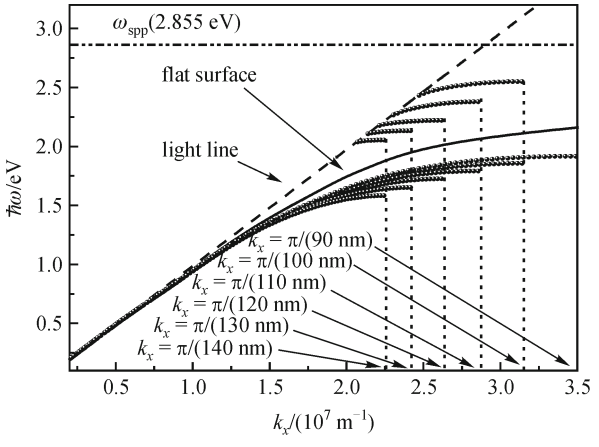

Fig. 11 Calculated dispersion curves for Cu-Si_3N_4 interface with sinusoidal shape with period a = 90–140 nm and depth $h = 0.1a$

observed that the lower branches are within the frequency range of Si-NCs while the higher branches are in the range of much higher frequencies. So if higher branches are desired for SPP enhancement, shorter grating wave vector ($\boldsymbol{K}_g$) is required to move the dispersion curve of higher branch to short wave vector range. In Fig. 3, the dispersion curve of SPP mode on flat interface is much closer to the light line as decreasing wave vector. It could be expected that higher branches would be also very close to the light line due to the nature that higher branches are always between the dispersion curve on flat interface and dielectric light line. Intuitively, the achievable SPP enhancement of high branches would be very low. Furthermore, it can also be understood as that the wavelength of such SPP mode is much longer (shorter wave vector) so that the advantage introduced from small mode volume of SPP mode is not so significant. For this consideration, the lower branch is more preferred to be applied in the interested frequency range. It should be mentioned that the higher branches can also be applied if the semiconductor materials with higher luminescence frequency, e.g., blue light region such as GaN or Si-NCs with very small averaged size are considered.

With a = 120 nm, the field intensity of H_y at BE-frequency were calculated and the results are shown in Fig. 12 in contour map, where all the intensity are normalized by the maximum value on boundary and the regions of high field strength are shown as white. As mentioned by Barnes, the physical origin of the SPP band gap can be found from the fact that two standing wave solutions of SPP modes take different positions with respect to the peaks and troughs of the interface [27]. Such indication can be observed clearly in Fig. 12. For the lower frequency mode (Fig. 12(a)), the surface charge distribution should be concentrated around the peaks so that extremum of normal field component occur at the same position, whereas the extremum of H_y and is around the toughs. For the higher frequency mode (Fig. 12(b)), H_y will occur at peaks.

After the dispersion curve and electromagnetic field distribution are obtained, the PF can be calculated in success [20,21]. Figure 13 is the calculated PF at BE-frequency for Cu-Si_3N_4 grating by setting a = 120 nm and $d = 0.1a$. The regions of high PFs are shown as white. As shown in Fig. 13, PF is related to the position of Si-NCs along both x and z axes. Especially, PF decays along z direction with $\boldsymbol{E}(x, z)$ so that significant SE enhancement can be achieved only near the interface. In order to evaluate the SPP enhancement conveniently with various periods of grating, we assume that the Si-NCs are uniformly distributed in dielectric layer and the PF is averaged within one period along x axis and one decay length D_z along z axis, which denotes the length when the electric field decay to the 1/e of that at interface $z = s(x)$, in the dielectric:

$$\mathrm{PF}_{\mathrm{avg}}(x,z) = \frac{1}{a}\frac{1}{D_z}\int_0^a\int_0^{D_z}\mathrm{PF}(x,z)\mathrm{d}z\mathrm{d}x. \tag{9}$$

In the followed parts, the averaged PF is used for discussion. Obviously, D_z should be replaced by the thickness of the active layer for a real device.

In our previous work [20,21], it has been demonstrated that Au, Ag Al and Cu-Si_3N_4 gratings can be used to enhance the SE of Si-NC with proper period. Here we re-plot those results in Fig. 14. It can be seen that obvious enhancement are achieved within the frequency range of Si-NCs luminescence with the Au Cu, Ag and Al-Si_3N_4 grating. Especially for Cu-Si_3N_4 gratings, as the period is varied from 90 to 140 nm, the BE-frequency is decreased from $\hbar\omega = 1.92$ to 1.58 eV while the related

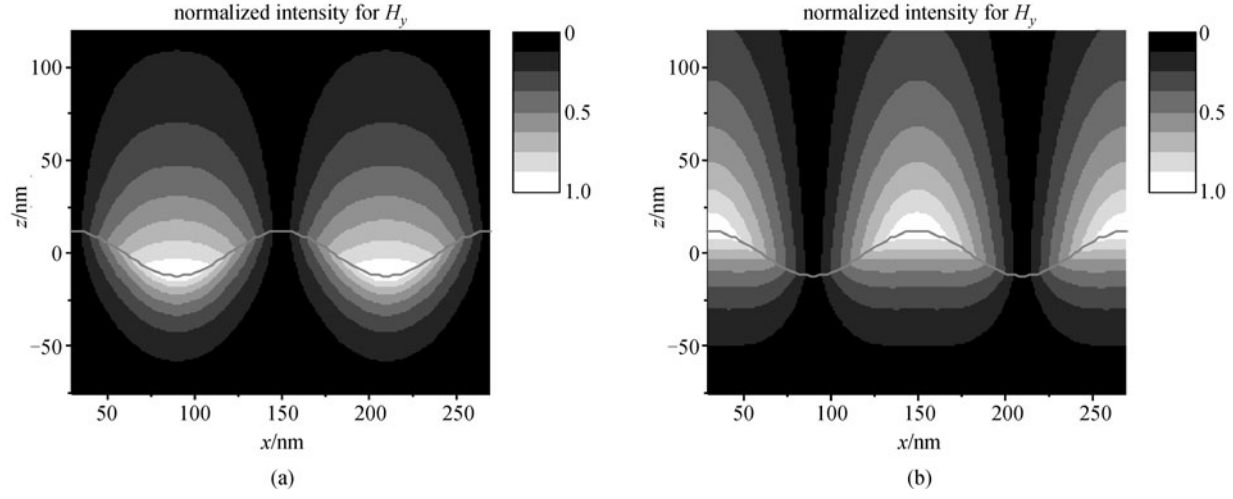

Fig. 12 Normalized spatial distribution of magnetic field normal to symmetry $|H_y|$: (a) for low frequency mode; (b) high frequency mode at BE-frequency. The regions of high field strength are shown as white

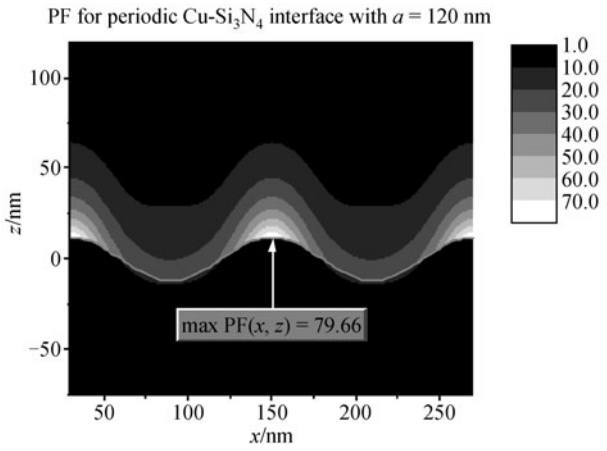

Fig. 13 Calculated PF distribution for Cu-Si_3N_4 grating within range of 30 nm$\leqslant x \leqslant$270 nm and –120 nm$\leqslant z \leqslant$120 nm by setting a = 120 nm and $d = 0.1a$. Regions of high PFs are shown as white

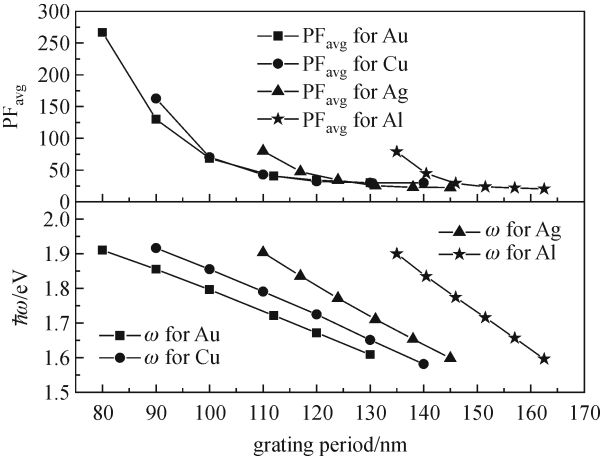

Fig. 14 Calculated max PF_{avg} and related BE-frequency versus various period for sinusoidal shaped Au, Cu, Ag and Al-Si_3N_4 interface with $d = 0.1a$

maximum PF_{avg} is from 162.7 to 29.8. The SPP resonant frequencies for flat Au, Cu, Ag and Al-Si_3N_4 interface are $\hbar\omega = 2.38$, 2.85, 3.15 and 4.73eV, all of which are higher than the energy of Si-NCs luminescence. Then it can be concluded that with proper setting grating period, metallic grating can be applied to overcome the mismatch between metal SPP resonant frequency and luminescence frequency of Si-NCs in spite of the applied metal materials. Meanwhile, it can be also found that both the BE-frequency and related maximum PF_{avg} decreases as the period increased for all four cases. It could be understood that higher PF is achieved at high frequency since shorter period is corresponding to longer wave-vector and closer to the SPP resonant frequency. With the same reason, it is also can be understood why the shorter period and higher maximum PF_{avg} can be achieved by such metal with relatively lower SPP resonant frequency. Since Au and Ag are not compatible with Si IC manufacturing and the SPP resonance frequency of Al is rather high, it could be expected that Cu-gratings are more suitable to enhance the SE of Si emitters applied on chip.

After the PF obtained, the enhanced internal QE η_{int} can be evaluated by Eq. (8). For more clarity, the original QE $\eta_o \left(\eta_o = \dfrac{\tau_r^{-1}}{\tau_r^{-1} + \tau_{nr}^{-1}}\right)$ is also calculated for comparison. The η_{int} are calculated in the range of $20 < PF < 160$ (according to the average PF of Cu-Si_3N_4 gratings) and $1\% < \eta_o < 60\%$. The results for $1\% < \eta_o < 10\%$ and $10\% < \eta_o < 60\%$ are shown in Figs. 15(a) and 15(b), respectively.

From Fig. 15, significant QE improvement can be observed. In the lower η_o (1%–10%) range, the enhanced QE η_{int} can achieve the value of about 30%–94% as shown Fig. 15(a). For example, with setting $\eta_o = 3\%$ and PF = 40, η_{int} can be calculated as high as 55.3%. With higher (10%–60%), it is found that the η_{int} is very close to 100%. For example, with $\eta_o = 20\%$ and PF = 40, the value of η_{int} is 91%. These results indicate that radiative recombination

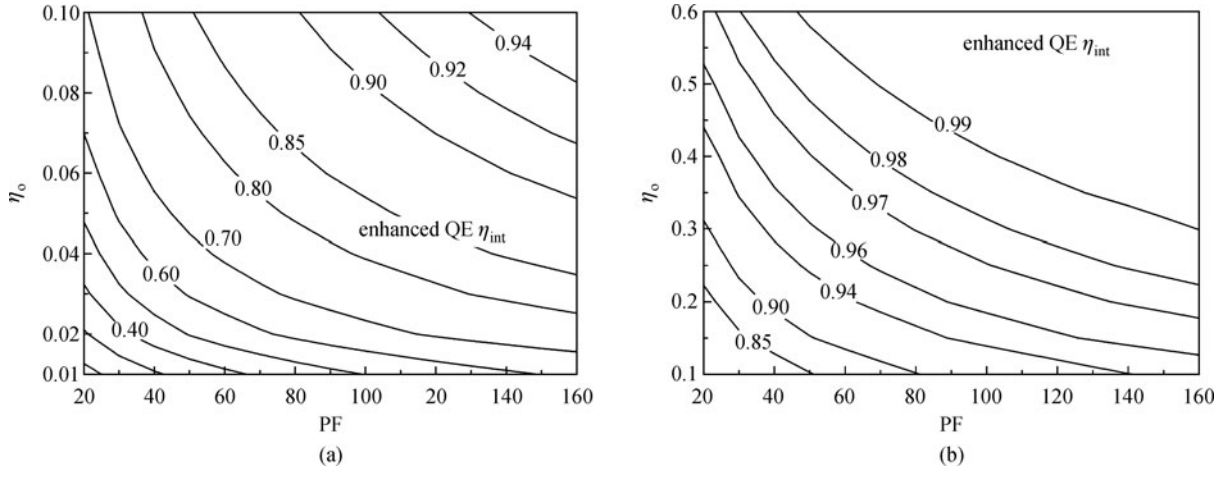

Fig. 15 Enhanced QE η_{int} versus various PF and original QE η_o for (a) $1\% < \eta_o < 10\%$ and (b) $10\% < \eta_o < 60\%$

dominates over the active region, even with a very low original QE ($< 10\%$), which is not difficult to reach.

In conclusion, the SE rate could be enhanced due to SPPBG on metallic gratings. With proper grating period, the BE-frequency of SPPBG can be engineered within luminescent frequency range of Si-NCs ($\hbar\omega = 1.6 - 1.9$ eV). The maximum PFs for Cu-Si_3N_4 gratings with 1μm width are calculated as 29.8–162.7. These results indicate that the Cu grating can be employed to overcome the frequency mismatch between SPP resonance and Si-NCs luminescence. Since Cu is the most commonly adopted metal in integrated-circuit manufacturing, this work provide a promising approach to realize Si light emitter on chip.

6 Conclusions

Aiming at improve the SE rate of nano-structured Si with SPP enhancement, we have proposed several approaches. The first one is based on metal-rich Au$(1-\alpha)$-$SiO_2(\alpha)$ cermet nanowaveguide. By properly choosing the component of the cermet, the dispersion of such SPP WG can be engineered so that the SE rate is greatly enhanced. For example, the PF of 210 is achieved with doping 20% SiO_2 at photon frequency of 1.718 eV (equivalent to the wavelength at 720 nm). Due to the evanescent field nature of SPP mode, we proposed double-layer SPP WG to achieve higher PFs since the electromagnetic field could be concentrated more in the active layer comparing with mono-layer SPP WG. The second one is introducing an Ag-poor cermet layer into SPP WG structure which is so-called compound layer structure. Due to large permittivity of Ag-poor cermet and its unique dispersion characteristic, DOS can be enhanced at the frequency much lower than the plasmon frequency of Ag. By properly choosing the component of the Ag-poor cermet, the SPP resonance can be engineered so that significant QE enhancement of Si-NC can be realized by using Ag instead of Au. The third one is based on SPPBG effect on metallic grating metallic grating. The calculated results indicate that the common metals such as Au, Ag, Al and Cu can be used to enhance the SE rate of Si-NCs with grating structure. It should be noticed that that the Cu grating can be employed. With the help of Cu-Si_3N_4 gratings, the BE-frequency of SPPBG can be engineered within luminescent frequency range of Si-NCs ($\hbar\omega = 1.6 - 1.9$ eV, equivalent to the wavelength of 775–652 nm). The maximum PFs are calculated as 29.8–162.7 with grating width of 1 μm. Since Cu is the most commonly adopted metal in integrated-circuit manufacturing, this is provide a promising approach to realize Si light sources on chip. Furthermore, the aforementioned three kinds of methods for SPP enhanced SE rate from Si-NCs show potential in developing high efficiency electric pump Si based light sources. The related work is undergoing and will be published elsewhere.

Acknowledgements This work was supported by the National Basic Research Program of China (No. 2011CBA00600 and 2007CB307004) and the National Natural Science Foundation of China (Grant Nos. 60877023, 61036010, 61036011, and 61107050). The authors would like to thank Xuan Tang, Weiwei Ke, Wei Zhang and Jiangde Peng for their valuable discussions and helpful comments.

References

1. Daldosso N, Pavesi L. Nanosilicon photonics. Laser & Photonics Reviews, 2009, 3(6): 508–534
2. Canham L T. Silicon quantum wire array fabrication by electrochemical and chemical dissolution of wafers. Applied Physics Letters, 1990, 57(10): 1046–1048
3. Qin G G, Li Y J. Photoluminescence mechanism model for oxidized porous silicon and nanoscale-silicon-particle-embedded silicon oxide. Physical Review B: Condensed Matter and Materials Physics, 2003, 68(8): 085309
4. Franzò G, Priolo F, Coffa S, Polman A, Carnera A. Room temperature electroluminescence from Er-doped crystalline silicon. Applied Physics Letters, 1994, 64(17): 2235–2237
5. Rong H S, Liu A, Jones R, Cohen O, Hak D, Nicolaescu R, Fang A, Paniccia M. An all-silicon Raman laser. Nature, 2005, 433(7023): 292–294
6. Kovalev D, Heckler H, Ben-Chorin M, Polisski G, Schwartzkopff M, Koch F. Breakdown of the *k*-conservation rule in Si nanocrystals. Physical Review Letters, 1998, 81(13): 2803–2806
7. Godefroo S, Hayne M, Jivanescu M, Stesmans A, Zacharias M, Lebedev O I, Van Tendeloo G, Moshchalkov V V. Classification and control of the origin of photoluminescence from Si nanocrystals. Nature Nanotechnology, 2008, 3(3): 174–178
8. Bianucci P, Rodríguez J R, Clements C M, Veinot J G C, Meldrum A. Silicon nanocrystal luminescence coupled to whispering gallery modes in optical fibers. Journal of Applied Physics, 2009, 105(2): 023108
9. Wilson W L, Szajowski P F, Brus L E. Quantum confinement in size-selected, surface-oxidized silicon nanocrystals. Science, 1993, 262(5137): 1242–1244
10. Pavesi L, Dal Negro L, Mazzoleni C, Franzò G, Priolo F. Optical gain in silicon nanocrystals. Nature, 2000, 408(6811): 440–444
11. Gontijo I, Boroditsky M, Yablonovitch E, Keller S, Mishra U, DenBaars S. Coupling of InGaN quantum-well photoluminescence to silver surface plasmons. Physical Review B: Condensed Matter and Materials Physics, 1999, 60(16): 11564–11567
12. Okamoto K, Niki I, Shvartser A, Narukawa Y, Mukai T, Scherer A. Surface-plasmon-enhanced light emitters based on InGaN quantum wells. Nature Materials, 2004, 3(9): 601–605
13. Sun G, Khurgin J B, Soref R A. Practicable enhancement of spontaneous emission using surface plasmons. Applied Physics Letters, 2007, 90(11): 111107
14. Khurgin J B, Sun G, Soref R A. Enhancement of luminescence

efficiency using surface plasmon polaritons: figures of merit. Journal of the Optical Society of America B, Optical Physics, 2007, 24(8): 1968–1980

15. Lai C W, Au J, Ong H C. Surface-plasmon-mediated emission from metal-capped ZnO thin film. Applied Physics Letters, 2005, 86(25): 251105
16. Purcell E M. Spontaneous emission probabilities at radio frequencies. Physical Review, 1946, 69(1946): 681
17. Hu X L, Huang Y D, Zhang W, Peng J D. Dominating radiative recombination in a nanoporous silicon layer with a metal-rich Au($1-\alpha$)-SiO_2(α) cermet waveguide. Applied Physics Letters, 2006, 89(8): 081112
18. Tang X, Wang Y X, Ke W W, Feng X, Huang Y D, Peng J D. Internal quantum efficiency enhancement of silicon nanocrystals using doublelayer Au-rich cermet films. Optics Communications, 2010, 283(13): 2754–2757
19. Tang X, Huang Y D, Wang Y, Zhang W, Peng J. Tunable surface plasmons for emission enhancement of silicon nanocrystals using Ag-poor cermet layer. Applied Physics Letters, 2008, 92(25): 251116
20. Feng X, Liu F, Huang Y D. Calculated plasmonic enhancement of spontaneous emission from silicon nanocrystals with metallic gratings. Optics Communications, 2010, 283(13): 2758–2761
21. Feng X, Liu F, Huang Y D. Spontaneous emission rate enhancement of silicon nanocrystals by plasmonic band gap on copper grating. Journal of Lightwave Technology, 2010, 28(9): 1420–1430
22. Zayatsa A V, Smolyaninovb I I, Maradudinc A A. Nano-optics of surface plasmon polaritons. Physics Reports, 2005, 408(3–4): 131–314
23. Spanier J E, Herman I P. Use of hybrid phenomenological and statistical effective-medium theories of dielectric functions to model the infrared reflectance of porous SiC films. Physical Review B: Condensed Matter, 2000, 61(15): 10437–10450
24. Barnes W L, Kitson S C, Preist T W, Sambles J R. Photonic surfaces for surface-plasmon Polaritons. Journal of the Optical Society of America A, 1997, 14(7): 1654–1661
25. Chandezon J, Dupuis M T, Cornet G, Maystre D. Multicoated gratings: a differential formalism application in the entire optical region. Journal of the Optical Society of America, 1982, 72(7): 839–846
26. Feng X, Ke W W, Tang X, Huang Y D, Zhang W, Peng J D. Numerical solution of surface plasmon polariton mode propagating on spatially periodic metal-dielectric interface. Journal of the Optical Society of America B, 2009, 26(12): B11–B20
27. Barnes W L, Preist T W, Kitson S C, Sambles J R. Physical origin of photonic energy gaps in the propagation of surface plasmons on gratings. Physical Review B: Condensed Matter and Materials Physics, 1996, 54(9): 6227–6244